Antiviral Research 211 (2023) 105541

Contents lists available at ScienceDirect

Antiviral Research

journal homepage: www.elsevier.com/locate/antiviral

Development of highly effective LCB1-based lipopeptides targeting the spike receptor-binding motif of SARS-CoV-2

Yuanmei Zhu [a,1], Min Li [b,1], Nian Liu [a,1], Tong Wu [a], Xuelian Han [b], Guangyu Zhao [b,**], Yuxian He [a,*]

[a] NHC Key Laboratory of Systems Biology of Pathogens, Institute of Pathogen Biology and Center for AIDS Research, Chinese Academy of Medical Sciences and Peking Union Medical College, Beijing, 100730, China

[b] State Key Laboratory of Pathogen and Biosecurity, Institute of Microbiology and Epidemiology, Academy of Military Medical Sciences, Beijing, 100071, China

ARTICLE INFO

Keywords:
SARS-CoV-2
LCB1
Resistance
Lipopeptide
Antivirals

ABSTRACT

LCB1 is a computationally designed 56-mer miniprotein targeting the spike (S) receptor-binding motif of SARS-CoV- 2 with high potent activity (Science, 2020; Cell host microbe, 2021); however, recent studies have demonstrated that emerging SARS-CoV-2 variants are highly resistant to LCB1's inhibition. In this study, we first identified a truncated peptide termed LCB1v8, which maintained the high antiviral potency. Then, a group of lipopeptides were generated by modifying LCB1v8 with diverse lipids, and of two lipopeptides, the C-terminally stearicacid-conjugtaed LCB1v17 and cholesterol-conjugated LCB1v18, were highly effective in inhibiting both S protein-pseudovirus and authentic SARS-CoV-2 infections. We further showed that LCB1-based inhibitors had similar α-helicity and thermostability in structure and bound to the target-mimic RBD protein with high affinity, and the lipopeptides exhibited greatly enhanced binding with the viral and cellular membranes, improved inhibitory activities against emerging SARS-CoV-2 variants. Moreover, LCB1v18 was validated with high preventive and therapeutic efficacies in K18-hACE2 transgenic mice against lethal SARS-CoV-2 challenge. In conclusion, our studies have provided important information for understanding the structure and activity relationship (SAR) of LCB1 inhibitor and would guide the future development of novel antivirals.

1. Introduction

As of October 6, 2022, the global pandemic of coronavirus disease 2019 (COVID-19) has resulted in ~617 million confirmed cases, including more than 6.5 million deaths (https://covid19.who.int/). Although over 12.6 billion vaccine doses have been administered, SARS-CoV-2 continues to spread with evolutionary mutations, leading to the emergence of many variants with significantly changed infectivity and pathogenesis (Callaway, 2021; Garcia-Beltran et al., 2021; He et al., 2021; Hoffmann et al., 2021; Kuzmina et al., 2021; Saito et al., 2022). As defined by the World Health Organization (WHO), there are currently five variants of concern (VOCs), including Alpha (B.1.1.7), Beta (B.1.351), Gamma (P.1), Delta (B.1.617.2), and Omicron (B.1.1.529), and seven variants of interest (VOIs), including Eta (B.1.525), Iota (B.1.526), Kappa (B.1.617.1), Lambda (C.37), B.1.617–3, Zeta (P.2), and Mu (B.1.621). Among divergent variants, Omicron emerged with the largest number of mutations in November 2021, and it has now evolved into several sublineages to dominate the worldwide pandemic (Shrestha et al., 2022).

Like other coronaviruses (CoVs), the spike (S) protein of SARS-CoV-2 not only plays a central role in viral infection through mediating the cell receptor binding and membrane fusion steps, it is also a major antigen to induce neutralizing antibodies (Walls et al., 2020; Wrapp et al., 2020); thus, the rapid emergence of various variants poses great challenges to the efficacies of S protein-targeting vaccines and antibody therapy. Previous studies demonstrated that the S protein mutations, especially in the receptor-binding domain or motif (RBD/RBM), can greatly affect the antibody binding and neutralization capacity (Bowen et al., 2022; Wang et al., 2021; Zhang et al., 2021). To develop inhibitors that can block the early entry step of infection, Cao and coworkers generated a group of miniproteins by using a computational *de novo* design approach, which could mimically bind to the RBM sequences with high

* Corresponding author.
** Corresponding author.
E-mail addresses: guangyu0525@163.com (G. Zhao), yhe@ipb.pumc.edu.cn (Y. He).
[1] These authors contributed equally to this work.

https://doi.org/10.1016/j.antiviral.2023.105541
Received 6 October 2022; Received in revised form 7 January 2023; Accepted 12 January 2023
Available online 20 January 2023

affinities thus blocking the interaction between the S protein and angiotensin-converting enzyme 2 (ACE2) efficiently (Cao et al., 2020). As expected, the miniproteins, including a 56-amino acid lead miniprotein termed LCB1, exhibited highly potent antiviral activity, and LCB1-based derivatives effectively blocked SARS-CoV-2 infection in human ACE2 (hACE2)-expressing transgenic mice when administrated as both pre-exposure prophylaxis and post-exposure therapy (Case et al., 2021). Unfortunately, several recent studies have indicated that SARS variants can display high resistance to LCB1's inhibition, thus challenging its potential as a candidate for drug development (Hunt et al., 2022; Javanmardi et al., 2021; Wu et al., 2022). Our results revealed that the Beta, Gamma, and Omicron variants caused high LCB1 resistance, whereas the Alpha, Delta, and Lambda variants were mildly resistant to the inhibition (Wu et al., 2022). Furthermore, we identified that substitutions of K417N, E406Q, L455F and N501Y in RBD critically determined the resistance phenotype (Wu et al., 2022). Therefore, here we devoted to develop novel LCB1-based inhibitors that could overcome the resistance problem. As results, we found that truncated LCB1-based lipopeptides possessed highly potent activities against SARS-CoV-2 and emerging variants.

2. Materials and methods

2.1. Plasmids and cells

Plasmids encoding the mutant S proteins of SARS-CoV-2 (Alpha, Beta, Gamma, Delta, Lambda, and Omicron) were a kind gift from Linqi Zhang at the Tsinghua University (Beijing, China). Plasmids encoding a panel of mutant S proteins with single, double or triple mutations and 293T/ACE2 cells stably expressing human ACE2 were constructed in our laboratory and used in the previous studies (Yu et al., 2021a; Zhu et al., 2022a). HEK293T and Huh-7 cells were purchased from the American type culture collection (ATCC) (Rockville, MD, USA). Cells were cultured in complete growth medium consisting of Dulbecco's minimal essential medium (DMEM) supplemented with 10% fetal bovine serum (FBS), 100 U/ml of penicillin-streptomycin, 2 mM L-glutamine, and 1 mM sodium pyruvate under 5% CO_2 and 37 °C.

2.2. Synthesis of peptides and lipopeptides

LCB1 and its truncated peptides (LCB1v1∼ LCB1v13) were synthesized on rink amide 4-methylbenzhydrylamine (MBHA) resin using a standard solid-phase 9-flurorenylmethoxycarbonyl (FMOC) protocol as described previously (Yu et al., 2021a). The N-terminally conjugated lipopeptides (LCB1v14, LCB1v15, and LCB1v16) were generated by directly linking stearicacid (SA), linoleicacid (LA) or a cholesterol (Chol) molecule to the N-terminal amino group of the peptide chain. To prepare C-terminally stearicacid-conjugated lipopeptides (LCB1v17, LCB1v19, and LCB1v21), the template peptide contained a C-terminal lysine with a 1-(4,4-dimethyl-2,6-dioxocyclohexylidene)ethyl (Dde) side chain-protecting group, enabling the conjugation of stearicacid that requires a deprotection step in a solution of 2% hydrazine hydrate-*N, N*-dimethylformamide (DMF). The C-terminally Cholesterol-conjugated lipopeptides (LCB1v18, LCB1v20, and LCB1v22) were prepared by amidation of a C-terminal lysine side chain with cholesteryl succinate monoester. The lipopeptides were synthesized with or without a flexible 8-unit or 4-unit polyethylene glycol (PEG8 or PEG4) linker as described previously (Yu et al., 2021a). All the peptides and lipopeptides were acetylated at the N-terminus prior to resin cleavage, followed by purification by reverse-phase high-performance liquid chromatography (HPLC) to greater than 95% homogeneity and characterized with mass spectrometry.

2.3. Inhibition of pseudovirus infection

The inhibitory activities of peptides or lipopeptides on diverse SARS-CoV-2 pseudoviruses were measured by a single-cycle infection assay as described previously (Yu et al., 2021a). Briefly, pseudoviruses were packaged by cotransfecting HEK293T cells with an S protein-expressing plasmid and pNL4-3.luc.RE plasmid encoding an Env-defective HIV-1_{NL4-3} genome with luciferase reporter. Cell supernatants containing pseudovirus particles were collected after transfection 48 h and stored at −80 °C. A serially three-fold diluted peptide or lipopeptide was incubated with an equal volume of pseudoviruses at 37 °C for 1 h, and the inhibitor-virus mixture was then added to 293T/ACE2 or Huh-7 target cells at a density of 10^4 cells/100 μl per well in a 96-well culture plate. After incubation at 37 °C for 48 h, cells were harvested, lysed in reporter lysis buffer, and measured for luciferase activity using luciferase assay reagents and a luminescence counter (Promega, Madison, WI, USA).

2.4. Inhibition of live SARS-CoV-2 infection

The inhibitory activities of four representative inhibitors (LCB1, LCBv8, LCB1v17, and LCB1v18) against authentic SARS-CoV-2 (Wuhan-Hu-1 strain) infection were determined as described previously (Yu et al., 2021a; Zhu et al., 2022a). Brief, a serially three-fold diluted peptide or lipopeptide was incubated with 0.1 multiplicity of infection (MOI) of live wild-type (WT) virus at 37 °C for 1 h, and the inhibitor-virus mixture was then added into Vero E6 cells that were seeded in a 96-well plate one day before infection at a concentration of 1 × 10^4 cells/well. After 1 h incubation, cell supernatants were replaced with opti-MEM containing 1% bovine serum albumin (BSA) and cultured at 37 °C for 24 h. Next, the supernatants were collected for viral RNA extraction with a Direct-zol RNA MiniPrep kit (Zymo Research, CA, USA). Viral RNA copies were measured by real-time RT-PCR using primers and probe targeting the specific N gene. PCR amplification conditions were 50 °C, 15 min, 95 °C, 3 min; 95 °C, 15 s, 60 °C, 45 s + Plate Read, 50 cycles. The viral copy numbers (VCN) were calculated according to the standard curve, and percent inhibition was obtained by dividing the number of copies of the virus in the vehicle control group.

2.5. Cytotoxicity of LCB1-based inhibitors

The cytotoxicity of LCB1-based peptides or lipopeptides was measured on 293T/ACE2, Huh-7, and Vero E6 cells using Cell-Counting Kit-8 (Abbkine, Wuhan, China). In brief, cells were seeded on a 96-well tissue culture plate (1 × 10^4 cells per well), and 50 μl volumes of inhibitors at graded concentrations were added to the cells. After incubation at 37 °C for 48 h, 20 μl of CCK-8 solution was added into each well and incubated 2 h at 37 °C. Absorbance at 450 nm was measured using a Multiskan MK3 microplate reader (Thermo Fisher Scientific, Waltham, MA, USA), and percentage of cell viability was calculated.

2.6. Circular dichroism spectroscopy

The α-helicity and thermostability of LCB1-based inhibitors were determined by circular dichroism (CD) spectroscopy as described previously (Zhu et al., 2020). In brief, a peptide or lipopeptide was dissolved in phosphate-buffered saline (PBS; pH 7.2) with a final concentration of 20 μM and incubated at 37 °C for 30 min. CD spectra were obtained on Jasco spectropolarimeter (model J-815) a using a 1 nm bandwidth with a 1 nm step resolution from 195 to 270 nm at room temperature. The spectra were corrected by subtracting a solvent blank, and the α-helical content was calculated from the CD signal by dividing the mean residue ellipticity [θ] at 222 nm by with a value of −33,000 deg cm^2 $dmol^{-1}$ that corresponds to a 100% helix. Thermal denaturation was performed by monitoring the ellipticity change at 222 nm from 20 to 98 °C at a rate of 2 °C/min, and melting temperature (T_m) was defined as the midpoint of thermal unfolding transition.

2.7. Biolayer interferometry

The binding affinities of LCB1-based inhibitors to a target-mimic RBD protein were determined by biolayer interferometry (BLI). Briefly, a His-tagged recombinant RBD protein (Sino Biological, Beijing, China) was loaded on a NTA biosensor (ForteBio, San Francisco, CA, USA) at a concentration of 10 μg/ml for 120s in PBS, and a peptide or lipopeptide was gradient-diluted in PBS-T buffer (PBS plus 0.2% Tween 20). The binding kinetics was guided by associating in analyte substrates for 120s and disassociating in PBST alone for 300s.

2.8. Binding ability of peptide inhibitors with viral and cellular membranes

To determine the binding ability of inhibitors with the SARS-CoV-2 membrane, a polyethylene glycol (PEG) 6000-based method was used to separate the virus particles from the inhibitors as described previously (Zhu et al., 2019). In brief, a serially three-fold diluted peptide was incubated with an equal volume of D614G pseudovirus at 4 °C for 1 h. Then, 3% PEG 6000 was added to the virus and incubated 1 h at 4 °C. The mixture was centrifuged on a microcentrifuge at 14,000 rpm for 40 min, and the supernatants were removed. The virus pellet was washed two times with 1 ml of 3% PEG 6000 containing 10 mg/ml bovine serum albumin (BSA) and then resuspended in 100 μl of Dulbecco's modified Eagle medium (DMEM). The inhibitor-treated virus was mixed with 100 μl of Huh-7 cells (1×10^5/ml) to initiate the infection. After 48 h of culture, the inhibitory activity of the viral membrane-bound inhibitors was determined by luciferase assay reagents.

To determine the binding ability of inhibitors with the target cell membrane, Huh-7 cells were plated in a 96-well plate (10^4/well) and incubated at 37 °C overnight. An inhibitor was diluted and added to the cells and incubated 1 h at 37 °C. The cells were washed two times with PBS, followed by addition of D614G pseudovirus. After incubation at 37 °C for 48 h, the inhibitory activity of the inhibitors that survived the washing steps was measured by luciferase assay reagents.

2.9. Animal challenge experiment

The preventive and therapeutic efficacies of LCB1v18 were evaluated in an infection animal model as described previously (Sun et al., 2021). A total of 40 K18-hACE2 transgenic mice aged 6 ~ 8-weeks (GemPharmatech Co. Ltd., China) were kept in biosafety level-3 housing and given access to standard pellet feed and water ad libitum. All infectious experiments followed the standard operating procedures of the approved biosafety level-3 facility and were approved by the Animal Experiment Committee of Laboratory Animal Center, Institute of Microbiology and Epidemiology, AMMS (approval number: IACUC-IME-2021-017). Mice were intranasally inoculated with 1.5×10^3 PFU of SARS-CoV-2 (BetaCoV/Beijing/IMEBJ08/2020). The mice in prophylactic groups received nasal administration of LCB1v18 (3 mg/kg body weight) in 40 μl 2 h before challenge. The mice in therapeutic group were intranasally treated with the same amount of LCB1v18 (3 mg/kg) for 5 consecutive days from 2 h post challenge. Mice received normal saline as a sham. Body weight and survival of challenged mice were daily recorded within 14 days post challenge. On day 6 post challenge, lung tissues of 5 sacrificed mice in each group were harvested for further viral RNA loads measurement. Mice were anesthetized by intraperitoneal injection of sodium pentobarbital (100 mg/kg) prior to each nasal inoculation. Viral RNA in lung tissues was quantified by real-time RT-PCR. Briefly, total RNA in TRIzol (Ambion)-lysed lung tissues was extracted and reverse-transcribed to cDNA by using a reverse transcription kit (Takara, Japan). Subsequently, the viral copies targeting the E gene of SARS-CoV-2 were measured by real-time quantitative PCR using the following probe and primers: E_Sarbeco_P1: FAM-ACACTAGCCATCCTTACTGCGCTTCG-BBQ; E_Sarbeco_F: ACAGGTACGTTAATAGTTAATAGCGT; Sarbeco_R: ATATTGCAGCAGTACGCACACA.

2.10. Statistical analyses

The percent inhibition of virus infection and 50% inhibitory concentration (IC_{50}) of LCB1-based inhibitors were calculated using GraphPad Prism 6 software (GraphPad Software Inc., San Diego, CA, USA). Statistical comparison of survival curves was conducted using Log-rank (Mantel-Cox) test, and the statistical comparisons of viral loads in lung tissue and the inhibitory activities of membrane-bound inhibitors were conducted using Student's unpaired *t*-test. Significance of differences was set at $^*p < 0.05$, $^{**}p < 0.01$, and $^{***}p < 0.001$.

LCB1-based Inhibitors	Sequence structure	a.a.	Mean IC_{50} ± SD (nM)	
			293T/ACE2	Huh-7
LCB1	DKEWILQKIYEIMRLLDELGHAEASMRVSDLIYEFMKKGDERLLEEAERLLEEVER	56	0.21 ± 0.03	0.26 ± 0.06
Truncated peptides				
LCB1v1	EWILQKIYEIMRLLDELGHAEASMRVSDLIYEFMKKGDERLLEEAERLLEEVER	54	0.35 ± 0.24	0.41 ± 0.17
LCB1v2	LQKIYEIMRLLDELGHAEASMRVSDLIYEFMKKGDERLLEEAERLLEEVER	51	0.49 ± 0.22	0.58 ± 0.39
LCB1v3	QKIYEIMRLLDELGHAEASMRVSDLIYEFMKKGDERLLEEAERLLEEVER	50	31.93 ± 9.5	35.42 ± 16.7
LCB1v4	KIYEIMRLLDELGHAEASMRVSDLIYEFMKKGDERLLEEAERLLEEVER	49	803 ± 210.25	449.23 ± 201.3
LCB1v5	IYEIMRLLDELGHAEASMRVSDLIYEFMKKGDERLLEEAERLLEEVER	48	242 ± 62.57	228.7 ± 25.31
LCB1v6	YEIMRLLDELGHAEASMRVSDLIYEFMKKGDERLLEEAERLLEEVER	47	776.23 ± 219.81	949.67 ± 175.24
LCB1v7	EIMRLLDELGHAEASMRVSDLIYEFMKKGDERLLEEAERLLEEVER	46	>20000	>20000
LCB1v8	LQKIYEIMRLLDELGHAEASMRVSDLIYEFMKKGDERLLEEAERLLEEV	49	0.24 ± 0.04	0.23 ± 0.02
LCB1v9	LQKIYEIMRLLDELGHAEASMRVSDLIYEFMKKGDERLLEEAERLLEE	48	0.8 ± 0.3	1.13 ± 0.42
LCB1v10	LQKIYEIMRLLDELGHAEASMRVSDLIYEFMKKGDERLLEEAERLLE	47	2.14 ± 0.29	1.39 ± 0.59
LCB1v11	LQKIYEIMRLLDELGHAEASMRVSDLIYEFMKKGDERLLEEAERLL	46	3.77 ± 0.28	3.57 ± 3
LCB1v12	LQKIYEIMRLLDELGHAEASMRVSDLIYEFMKKGDERLLEEAER	44	22.83 ± 13.22	27.43 ± 14.82
LCB1v13	LQKIYEIMRLLDELGHAEASMRVSDLIYEFMKKGDERLLEEA	42	29.72 ± 16.65	40.23 ± 19.82
Lipopeptides				
LCB1v14	SA-PEG_8-LQKIYEIMRLLDELGHAEASMRVSDLIYEFMKKGDERLLEEAERLLEEV	49	0.71 ± 0.34	1.55 ± 0.39
LCB1v15	LA-PEG_8-LQKIYEIMRLLDELGHAEASMRVSDLIYEFMKKGDERLLEEAERLLEEV	49	1.2 ± 0.11	1.14 ± 0.38
LCB1v16	Chol-PEG_8-LQKIYEIMRLLDELGHAEASMRVSDLIYEFMKKGDERLLEEAERLLEEV	49	0.97 ± 0.04	2.42 ± 0.14
LCB1v17	LQKIYEIMRLLDELGHAEASMRVSDLIYEFMKKGDERLLEEAERLLEEV-PEG_8-K(SA)	49	0.26 ± 0.01	0.2 ± 0.04
LCB1v18	LQKIYEIMRLLDELGHAEASMRVSDLIYEFMKKGDERLLEEAERLLEEV-PEG_8-K(Chol)	49	0.17 ± 0.02	0.12 ± 0.01
LCB1v19	LQKIYEIMRLLDELGHAEASMRVSDLIYEFMKKGDERLLEEAERLLEEV-PEG_4-K(SA)	49	0.42 ± 0.15	0.83 ± 0.25
LCB1v20	LQKIYEIMRLLDELGHAEASMRVSDLIYEFMKKGDERLLEEAERLLEEV-PEG_4-K(Chol)	49	0.66 ± 1.6	0.64 ± 0.25
LCB1v21	LQKIYEIMRLLDELGHAEASMRVSDLIYEFMKKGDERLLEEAERLLEEV-K(SA)	49	4.18 ± 1.79	11.8 ± 3.3
LCB1v22	LQKIYEIMRLLDELGHAEASMRVSDLIYEFMKKGDERLLEEAERLLEEV-K(Chol)	49	19.64 ± 13.64	21.12 ± 9.53

Fig. 1. Structural and functional characterization of LCB1-based inhibitors. For clarity, the sequence structures of truncated peptides (LCB1v1 ~ LCB1v13) and lipid-conjugated lipopeptides (LCB1v14 ~ LCB1v22) are illustrated, with four representative inhibitors (LCB1, LCB1v8, LCB1v17, and LCB1v18) marked in red. The inhibitory activities of LCB1-based inhibitors against wild-type SARS-CoV-2 pseudovirus infections on 293T/ACE2 or Huh-7 cells were determined by a single-cycle infection assay. The experiments were performed in triplicate and repeated three times, and the IC_{50} values are expressed as mean values ± standard deviation (SD).

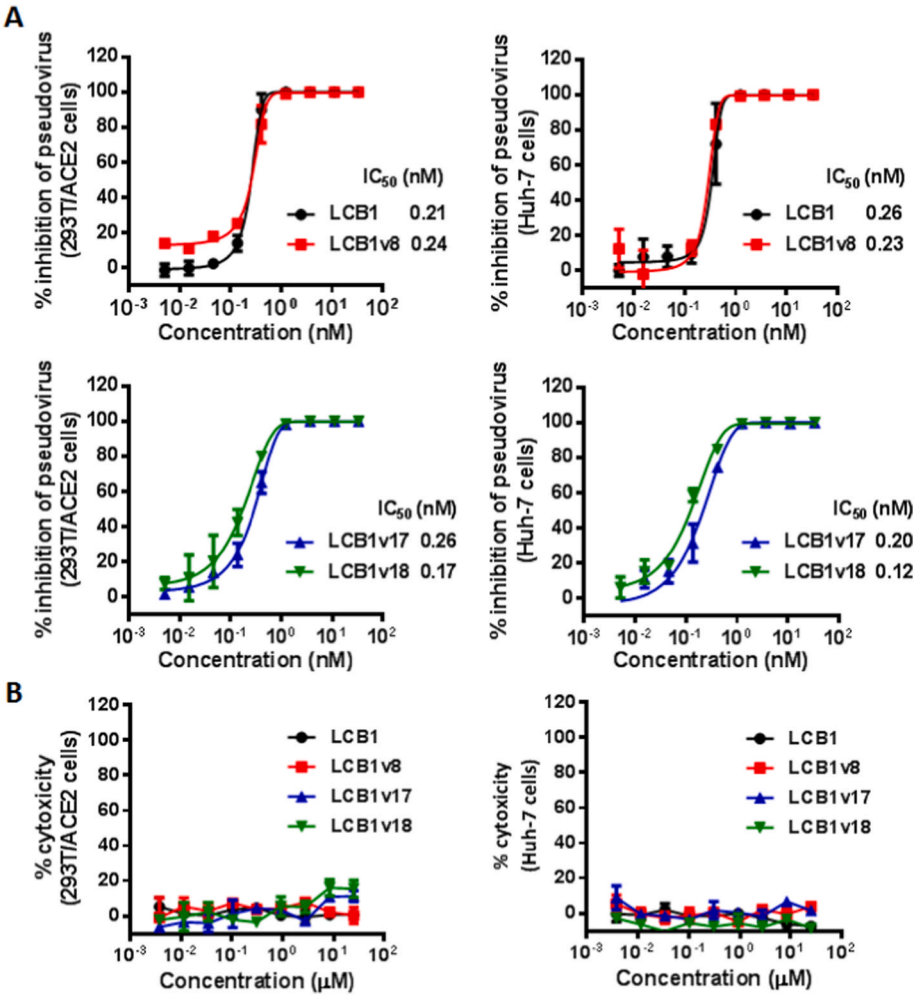

Fig. 2. The antiviral activity and cytotoxicity of LCB1 and its derivatives. (**A**) The inhibitory activities of four representative LCB1-based inhibitors (LCB1, LCB1v8, LCB1v17, and LCB1v18) were determined by the pseudovirus-based single-cycle infection assay. (**B**) The cytotoxicity of LCB1 and its derivatives was measured by Cell-Counting Kit-8. Data shown are from three independent experiments and presented as means ± SD.

3. Results

3.1. Identification of a truncated LCB1 peptide with similar antiviral activity

We recently reported the resistance profile and underlying mechanism of divergent SARS-CoV-2 variants to a peptide-based LCB1 inhibitor (Wu et al., 2022). In order to develop an effective inhibitor that can overcome the resistance problem, here we continued our efforts to characterize the structure and activity relationship (SAR) of LCB1 by truncation. As indicated by the peptides from LCB1v1 to LCB1v7 illustrated in Fig. 1, deletion of two or four N-terminal residues did not significantly affect the inhibitory activities of inhibitors; however, further N-terminal truncation resulted in dramatically reduced antiviral activities. By using the N-terminally truncated LCB1v2 peptide as a template, we found that two C-terminal residues could be further removed without impairing the inhibitory activity of the peptide, but deleting more residues from the C-terminal was not tolerable, as indicated by the peptides from LCB1v8 to LCB1v13 (Figs. 1 and 2). Therefore, LCB1v8 was initially identified as a minimal unmodified peptide, which could be used as a starting template for inhibitor optimization.

3.2. Development of lipopeptide-based inhibitors retaining the high potency

Our previous studies demonstrated that lipid conjugation could render peptide-based inhibitors with greatly improved antiviral activity, especially against those inhibitor-resistant viruses (Xue et al., 2022; Yu et al., 2021a; Zhu et al., 2022a). Importantly, comparing the unconjugated native peptides the lipopeptide-based inhibitors also exhibited sharply increased stability thus conferring an extended *in vivo* half-life. Herein, we modified LCB1v8 with diverse lipids through N- or C-terminal conjugation, thereby resulting in a panel of lipopeptides from LCB1v14 to LCB1v22 (Fig. 1). Similarly, the inhibitory activities of lipopeptides against the pseudovirus infections on 293T/ACE2 and Huh-7 cells were measured. It was found that all the lipopeptides from LCB1v14 to LCB1v20 maintained the highly potent antiviral activity, with LCB1v17 and LCB1v18 being the most effective inhibitors. Specifically, LCB1v17 and LCB1v18 inhibited the pseudoviruses with mean IC_{50} values of 0.26 nM and 0.17 nM on 293T/ACE2 cells and of 0.2 nM and 0.11 nM on Huh-7 cells (Figs. 1 and 2). In comparison, two C-terminally conjugated lipopeptides LCB1v21 and LCB1v22, which had no a flexible PEG linker between the peptide sequence and lipid molecule, exhibited obviously reduced antiviral potencies. None of LCB1-based inhibitors displayed appreciable cytotoxicity in 293T/ACE2

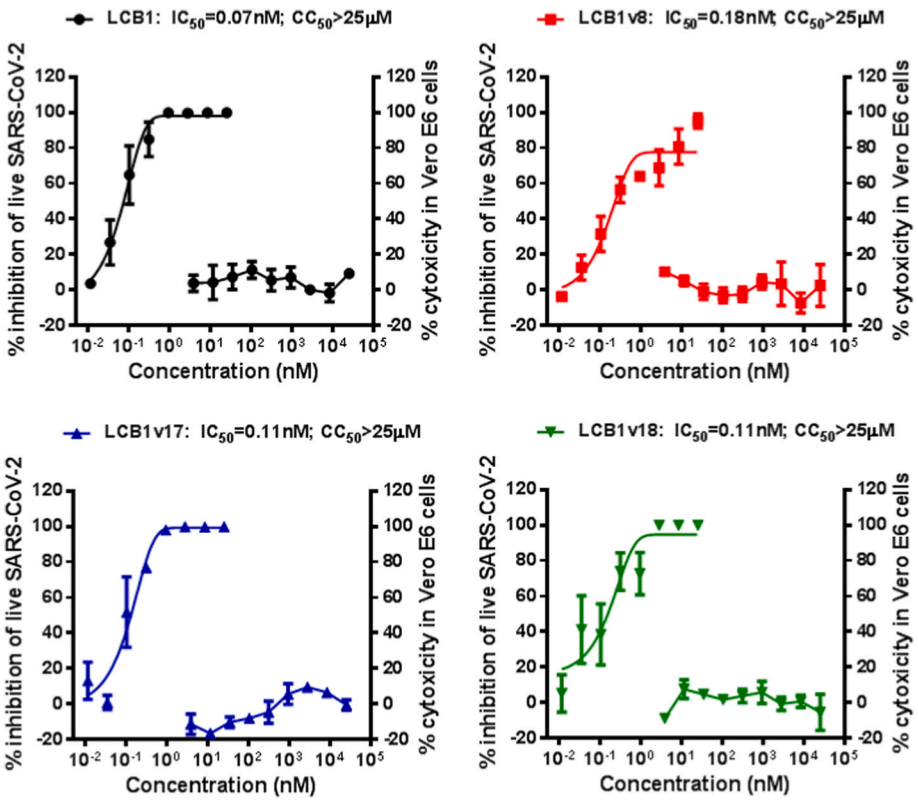

Fig. 3. Inhibitory activity of LCB1-based inhibitors against authentic SARS-CoV-2 infection. The inhibitory activities of LCB1 and its derivatives were determined with replicative SARS-CoV-2 (Wuhan-Hu-1 strain) on Vero E6 cells. The cytotoxicity of each inhibitor on Vero E6 cells was similarly measured by Cell-Counting Kit-8. Data shown are from three independent experiments and presented as means ± SD.

and Huh-7 cells at a concentration as high as 25 μM.

Next, we determined the activities of template peptides and two lipopeptides in inhibiting infection of replicative SARS-CoV-2 (Wuhan-Hu-1 strain). As shown in Fig. 3, while LCB1 and LCB1v8 inhibited SARS-CoV-2 infection in Vero cells with mean IC_{50} of 0.07 and 0.18 nM, respectively, LCB1v17 and LCB1v18 inhibited this authentic virus with mean IC_{50} of 0.11 and 0.11 nM, respectively. No cytotoxicity was found in Vero cells either.

3.3. Biophysical characterization of LCB1-based inhibitors

To know the structural properties of LCB1-based inhibitors, we first used CD spectroscopy to determine their secondary structure and thermal stability. As shown in Fig. 4A, the CD spectra of LCB1, LCBv8, LCB1v17, and LCB1v18 displayed typical double minima at 208 and 222 nm with similar α-helical contents (77–79%); however, their thermal unfolding transition could not be finely determined due to a melting temperature (T_m) greater than 95 °C. Subsequently, we applied biolayer interferometry (BLI) to measure the binding affinity of each inhibitor to a target-mimic RBD protein. As shown in Fig. 4B, LCB1 and LCBv8 peptides exhibited the equilibrium dissociation constants (Kd) of 2.64 and 6.11 nM, respectively, whereas LCB1v17 and LCB1v18 lipopeptides had Kd values of 0.34 and 1.83 nM, respectively. In addition, we demonstrated that the antiviral activities of LCB1-based inhibitors had no significant changes after they were stored at 4 °C, 25 °C or 37 °C for 6 weeks (Fig. 4C).

3.4. Cholesterylated inhibitors can efficiently bind to cellular and viral membranes

We previously demonstrated that cholesterol-conjugated fusion inhibitor lipopeptides can preferentially bind to both the viral and cellular membranes (Chong et al., 2018; Zhu et al., 2019). To further characterize the mechanism underlying the high potency of the LCB1-based lipopeptides, here we compared the membrane-binding abilities of LCB1 and LCB1v18. To determine the binding and inhibitory abilities of inhibitors with viral membrane, the inhibitors were preincubated with SARS-CoV-2 pseudoviruses, and the unbound ones were removed away by precipitating the viruses with PEG 6000. The antiviral activities of the virus-bound inhibitors were determined in Huh-7 cells by a single-cycle infection assay. As shown in Fig. 5A, LCB1 with the washsing step inhibited the viruses with a mean IC_{50} of 110.3 nM, which indicated a more than 1000-fold reduction in its antiviral activity; in contrast, LCB1v18 with and without washing exhibited IC_{50} values of 15.5 nM or 0.11 nM, which calculated a 141-fold difference.

Next, we sought to characterize the cell membrane-binding abilities of LCB1 and LCB1v18. For this, two inhibitors were preincubated with Huh-7 cells, followed by thorough washing to remove unbound inhibitors. The virus was then added to initiate infection, and the antiviral activities of the membrane-bound inhibitors that survived the washing steps were similarly determined. As shown in Fig. 5B, LCB1 also dramatically reduced its inhibitory activity, whereas the activity of LCB1v18 was largely sustanined. Taken together, these results suggested that LCB1v18 interacts preferentially with the viral and cellular membranes, thus raising the local concentration of the inhibitors to block the virus infecftion more efficiently.

3.5. LCB1v17 and LCB1v18 are highly potent inhibitors of SARS-CoV-2 variants

We were intrigued to know the inhibitory activities of LCB1-based lipopeptides against divergent SARS-CoV-2 variants. To this end, a

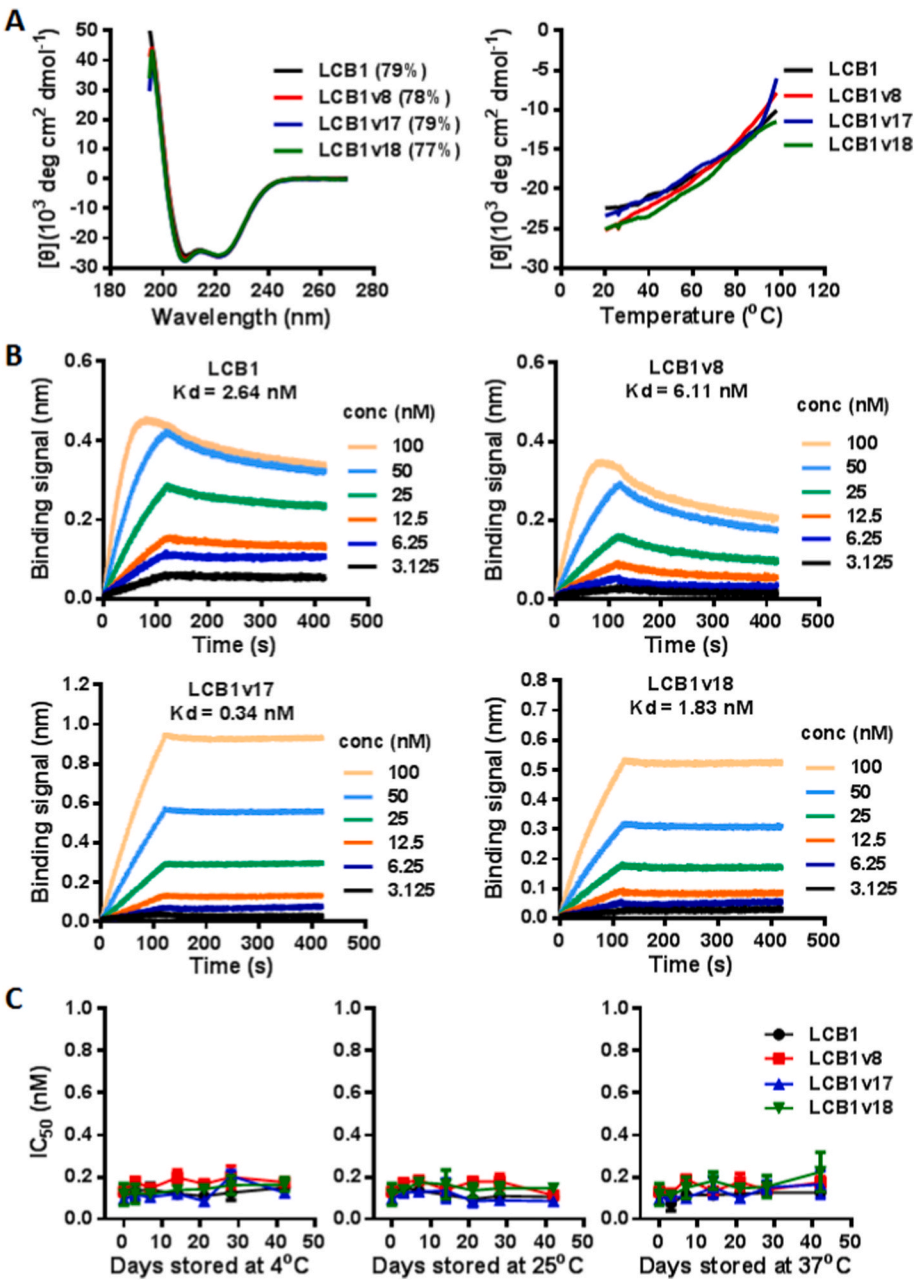

Fig. 4. Biophysical characterization of LCB1-based inhibitors. (**A**) The α-helicity (left panel) and thermostability (right panel) of LCB1, LCB1v8, LCB1v17 or LCB1v18 at 20 μM were determined by CD spectroscopy. (**B**) The binding affinity of each inhibitor with a target-mimic RBD protein was determined by biolayer interferometry (BLI), in which a His-tagged recombinant RBD protein was loaded onto an NTA biosensors and equilibrated before the baseline was set to zero at t = 0. The binding kinetics was guided by associating in different concentrations of an inhibitor for 120s and disassociating for 300s. The equilibrium dissociation constant (Kd) was calculated. (**C**) The pseudovirus-inhibitory activities of LCB1-based inhibitors after storing at different temperatures for 6 weeks were measured on 293T/ACE2 cells by a single-cycle infection assay. Data shown in (**A**–**B**) are representative of two independent experiments. Data shown in (**C**) are from three independent experiments and presented as means ± SD.

large panel of pseudoviruses corresponding to five VOCs and one VOI (Lambda) as well as various mutants was packaged and applied in the single-cycle infection assay. As shown in Table 1, LCB1v17 and LCB1v18 displayed greatly improved activities in inhibiting diverse LCB1-resistant viruses. For example, while LCB1 inhibited the Beta variant with IC_{50} values of 940.47 nM on 293T/ACE2 and 446.33 nM on Huh-7 cells, LCB1v17 and LCB1v18 generated the IC_{50} values of 40.41 nM and 18.25 nM on 293T/ACE2 and of 47.99 nM and 26.15 nM on Huh-7 cells, which indicated that the lipopeptides had a 9 – 52-fold increased potency than LCB1. In the inhibition of Omicron, LCB1 had the IC_{50} values of 925.4 nM on 293T/ACE2 and 712.17 nM on Huh-7, whereas LCB1v17 and LCB1v18 exhibited the IC_{50} values of 53.58 nM and 31.22 nM on 293T/ACE2 and of 51.9 nM and 26.67 nM, indicating a 14 – 30-fold increased potency for the lipopeptides over LCB1. Additionally, the two lipopeptides also demonstrated the advantages against the Gamma variant and the mutant of triple mutations and so on. As controls, a fusion-inhibitory lipoeptide IPB24 (Yu et al., 2021a; Zhu et al., 2022b), which is currently under clinical trails in China, exhibited potent, broad-spectrum inhibitory activities against all the tested muatants, whereas the combination therapy of two human neutralizing antibodies (BRII-196 and BRII-198), which has already been approved for the treatment of mild COVID-19 in patients (Group, 2022; Hoy, 2022), had a obviously decreased potency in inhibiting the Omicron variant.

3.6. LCB1v18 exhibits high prophylactic and therapeutic efficacies in K18-hACE2 mice

Based on the above results, the cholesterol-conjugated lipopeptide LCB1v18 behaved with the most active antiviral activity; thus, we evaluated its prophylactic and therapeutic effects in K18-hACE2 transgenic mice that infected with a lethal dose of SARS-CoV-2 (illustrated in Fig. 6A). In the prophylaxis experiment, 10 mice were intranasally

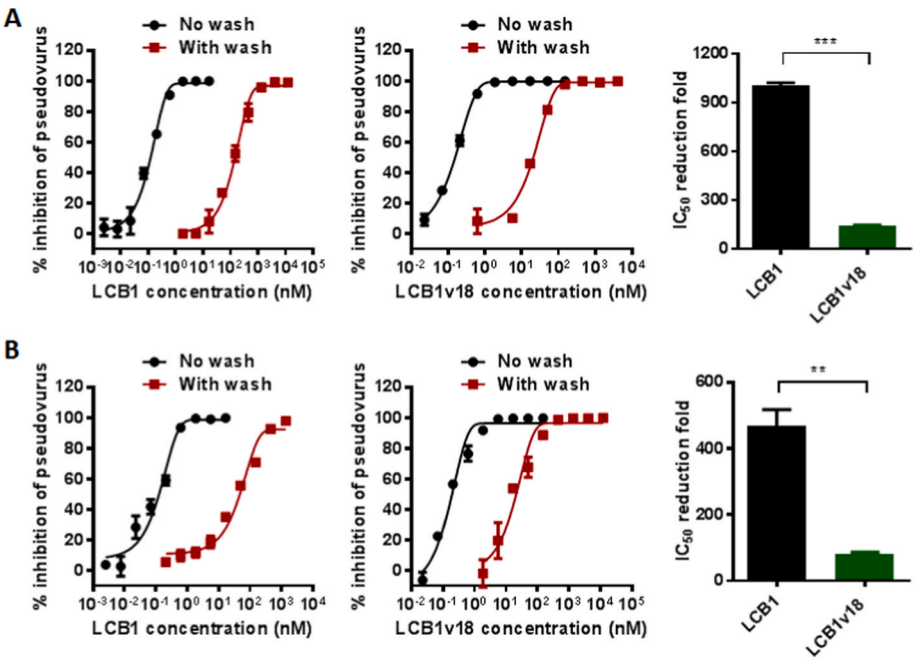

Fig. 5. Binding ability of LCB1-based inhibitors with viral and cellular membranes. LCB1 and LCB1v18 were pre-incubated with SARS-CoV-2/D614G pseudovirus or Huh-7 cells, followed by the washing step. The sustained antiviral activities of the virus-bound or cell-bound inhibitors were measured by a single-cycle infection assay, and the reduction folds of IC_{50} values were statistically compared. The experiments were repeated two times with consistent results, and representative data are shown.

administrated once with LCB1v18 2 h before challenge, and 10 mice in the therapy group received intranasal treatment of LCB1v18 once-daily for a total of 5 times. Saline was used as a control in the prevention and treatment experiments, respectively. On day 6 post-challenge, 5 mice per group were sacrificed and lung tissues were collected to assess viral loads and histopathological damages, and body weight changes and survival of other mice were recorded daily for 14 days post-challenge. As shown in Fig. 6, mice in the prophylaxis group obtained complete protection against lethal viral challenge, all mice survived (Fig. 6B) and their body weight steadily increased from day 3 (Fig. 6D). Although the therapy group showed a certain degree of weight loss in the middle of the 14-day period, it was able to recover later (Fig. 6E), which still enabled the mice to obtain a 60% survival rate against the lethal challenge (Fig. 6C). In contrast, control mice all died 5–7 days after challenge, accompanied by severe weight loss. These results suggest that LCB1v18 can inhibit SARS-CoV-2 infection *in vivo*, as confirmed by detection of lung viral loads. Mice receiving LCB1v18 before or after challenge showed significantly lower viral copies in lungs ($P < 0.01$) than that in control (Fig. 6 (F and G)). Further examination of associated histopathological changes illustrated that both prophylactic and therapeutic LCB1v18 administrations significantly alleviated lung injury caused by lethal SARS-CoV-2 infection (Fig. 6H). The LCB1v18-treated mice under lethal challenge exhibited fewer histopathological damages accompanied by little inflammatory cell infiltration (Fig. 6Hb), and no obvious histopathological change was observed in prophylactic-administered mice (Fig. 6Ha). In contrast, severe lung damage was observed in a control group of prophylactic or treated mice (Fig. 6Hc and d), which showed similar interstitial pneumonia characterized with lots of inflammatory cell infiltration, denaturation of alveoli epithelial cells, and quantities of erythrocytes (blue arrow) or collapsed bronchiolar epithelium cells (green arrow) in bronchiole tubes. Overall, LCB1v18 has potent prophylactic and therapeutic efficacies in protecting susceptible animal models against lethal SARS-CoV-2 challenge.

4. Discussion

In this study we first identified a truncated LCB1 peptide termed LCB1v8, which had a length of 49 amino acids but fully retained the potent antiviral activity of the parent peptide. A group of lipopeptides were accordingly created by conjugating LCB1v8 with various lipid molecules, with the C-terminally stericacid-modified LCB1v17 and cholesterol-modified LCB1v18 being the most active inhibitors in inhibiting both S protein-based pseudovirus and authentic SARS-CoV-2 infections. With CD spectroscopy and biolayer interferometry, we demonstrated that LCB1-based peptides and lipopeptides possessed similar α-helicity and thermostability and bound to the target-mimic recombinant RBD protein efficiently. As anticipated, the lipopeptides can preferentially bind to the viral and cellular membranes, which increase the local concentration of the inhibitors to block the virus infecftion more efficiently. Promisingly, LCB1-based lipopeptides possessed greatly improved activities against divergent emerging SARS-CoV-2 variants, and LCB1v18 exhibited very high efficacies when administrated as pre-exposure prevention and post-exposure treatment against lethal SARS-CoV-2 challenges in human ACE2-transgenic mouse models. In one-sentence conclusion, our studies have provided valuable information for understanding the structure and activity relationship of LCB1 inhibitor and would guide the rational design of novel antivirals for combating the COVID-19 pandemic.

Since the SARS-CoV-2 outbreak, we have dedicated to develop inhibitors that can efficiently block virus's entry step. As consequences, several membrane fusion-inhibitory lipopeptides were generated with highly potent activity against SARS-CoV-2 and emerging variants (Yu et al., 2021a, 2021b; Zhu et al., 2020, 2021, 2022a). Our previous studies demonstrate that a lipopeptide-based virus entry inhibitor has multiple advantages comparing to its unmodified parental peptide (Xue et al., 2022; Yu et al., 2021a; Zhu et al., 2019, 2020, 2022a). First, lipopeptides can bind to the viral and cell membranes, which greatly elevates the local concentration of the inhibitor thus enhancing the antiviral activity dramatically. Second, the lipid conjugation strategy does sharply increase the stability of a peptide drug thus conferring a significantly extended *in vivo* half-life. Third, the lipopeptide inhibitors can enable activity against virus entrance from both the cell surface and endosomal pathways (de Vries et al., 2021; Outlaw et al., 2020). After LCB1 inhibitor was first reported in September 2020 (Cao et al., 2020), it attracted our attention because of its design strategy as a peptide-like miniprotein and high antiviral potency by targeting the spike RBM to

Table 1
Inhibitory activity of LCB1-based lipopeptides and control inhibitors against divergent SARS-CoV-2 variants (IC_{50} ± SD) [a].

SARS-CoV-2	Pseudovirus on 293T/ACE2 cells					Pseudovirus on Huh-7 cells				
	LCB1	LCB1v17	LCB1v18	IPB24	BRII-196/198	LCB1	LCB1v17	LCB1v18	IPB24	BRII-196/198
D614G reference	0.05 ± 0.004	0.09 ± 0.01	0.1 ± 0.05	6.14 ± 1.24	46.13 ± 0.91	0.06 ± 0.01	0.08 ± 0.01	0.08 ± 0.02	3.19 ± 1.12	45.36 ± 4.26
Alpha	1.00 ± 0.06	0.75 ± 0.14	0.28 ± 0.01	5.81 ± 1.28	34.04 ± 9.76	0.74 ± 0.08	0.77 ± 0.15	0.32 ± 0.04	5.28 ± 1.76	47.64 ± 0.33
Beta	950.47 ± 69.76	40.41 ± 11.25	18.25 ± 0.65	5.66 ± 1.55	44.39 ± 20.97	446.33 ± 66.25	47.99 ± 0.09	26.15 ± 2.77	3.11 ± 0.23	34.33 ± 8.32
Gamma	204.5 ± 61.64	19.82 ± 2.53	10.85 ± 0.47	6.29 ± 1.45	50.32 ± 16.19	82.47 ± 16.78	18.22 ± 2.23	16 ± 1.74	4.01 ± 0.97	31.98 ± 3.17
Delta	0.66 ± 0.01	0.18 ± 0.01	0.22 ± 0.02	4.98 ± 1.04	47.34 ± 10.93	0.73 ± 0.19	0.53 ± 0.09	0.31 ± 0.01	3.33 ± 0.49	31.38 ± 5.58
Lamda	0.36 ± 0.01	0.17 ± 0.01	0.13 ± 0.01	6.55 ± 1.15	33.57 ± 6.73	0.49 ± 0.10	0.14 ± 0.02	0.11 ± 0.03	4.78 ± 1.55	22.70 ± 0.36
Omicron	925.40 ± 214.43	53.58 ± 0.18	31.22 ± 1.29	4.30 ± 0.36	763.13 ± 201.43	712.17 ± 305.38	51.9 ± 8.52	26.67 ± 5.28	2.41 ± 0.61	629.17 ± 109.60
Δ69-70	0.12 ± 0.02	0.11 ± 0.01	0.09 ± 0.001	3.73 ± 3.15	38.50 ± 13.16	0.14 ± 0.01	0.23 ± 0.01	0.21 ± 0.01	3.62 ± 1.03	38.29 ± 3.58
K417N	2.91 ± 0.35	4.75 ± 0.47	2.36 ± 0.49	6.03 ± 0.13	40.53 ± 6.86	4.65 ± 1.32	18.62 ± 3.42	5.6 ± 0.05	3.33 ± 0.30	39.56 ± 5.48
E484K	0.06 ± 0.01	0.11 ± 0.01	0.11 ± 0.01	5.37 ± 0.61	42.50 ± 4.49	0.08 ± 0.01	0.21 ± 0.01	0.19 ± 0.01	4.75 ± 0.45	31.75 ± 7.62
N501Y	0.21 ± 0.02	0.53 ± 0.04	0.38 ± 0.03	4.49 ± 0.25	34.39 ± 9.22	0.31 ± 0.03	1.25 ± 0.03	0.55 ± 0.01	3.87 ± 0.89	34.65 ± 7.44
P681H	0.07 ± 0.02	0.08 ± 0.01	0.13 ± 0.02	4.01 ± 1.17	42.94 ± 2.40	0.08 ± 0.004	0.25 ± 0.02	0.24 ± 0.01	2.02 ± 0.30	49.84 ± 7.93
Δ69–70/N501Y	0.21 ± 0.06	0.44 ± 0.1	0.28 ± 0.05	4.81 ± 1.14	42.94 ± 7.63	0.41 ± 0.02	1.11 ± 0.22	0.33 ± 0.02	4.83 ± 0.23	35.11 ± 1.53
E484K/N501Y	0.53 ± 0.14	0.66 ± 0.11	0.64 ± 0.01	4.73 ± 1.10	36.35 ± 3.72	0.63 ± 0.08	0.95 ± 0.1	0.62 ± 0.01	3.40 ± 1.28	37.91 ± 1.05
N501Y/P681H	0.19 ± 0.02	0.3 ± 0.02	0.18 ± 0.03	3.65 ± 0.26	34.93 ± 3.02	0.34 ± 0.01	1.27 ± 0.31	0.24 ± 0.04	2.55 ± 1.16	50.79 ± 0.95
Δ69–70/N501Y/P681H	0.17 ± 0.08	0.29 ± 0.01	0.10 ± 0.01	6.29 ± 0.64	37.17 ± 6.51	0.33 ± 0.05	1.38 ± 0.17	0.076 ± 0.017	5.19 ± 1.55	37.19 ± 0.10
K417N/E484K/N501Y	232.07 ± 108.63	37.15 ± 1.83	10.78 ± 1.6	6.10 ± 1.78	48.84 ± 8.14	327.1 ± 62.97	128.35 ± 10.54	35.74 ± 6.52	4.51 ± 0.85	23.92 ± 1.07
K417T/E484K/N501Y	58.52 ± 1.39	47.67 ± 1.13	18.86 ± 3.11	6.37 ± 1.11	57.73 ± 1.53	64.65 ± 16.78	56.06 ± 6.49	20.4 ± 0.43	3.77 ± 0.94	19.98 ± 1.43
L452R/T478K/P681R	0.15 ± 0.03	0.18 ± 0.01	0.13 ± 0.002	4.40 ± 1.00	32.57 ± 3.08	0.10 ± 0.03	0.15 ± 0.02	0.11 ± 0.02	2.99 ± 0.26	42.03 ± 7.92

[a] The experiments were performed in triplicate and repeated three times. The IC_{50} values of LCB1, LCB1v17, LCB1v18, and IPB24 are expressed at nM, whereas the IC_{50} values of BRII-196/198 are expressed at ng/ml, and the data are shown as means ± SD.

block the interaction between S protein and ACE2; thus, we have been working on the development of novel LCB1-based inhibitors with high enthusiasm. Given that LCB1 was computationally designed with 56 amino acids, which is not convenient for lipopeptide synthesis and large production, we began the optimization process by truncating the peptide sequences. As indicated by the truncated peptide LCB1v8, five N-terminal residues and two C-terminal residues of LCB1 were found not necessary for retaining the inhibitory potency. This truncation process has not only offered an ideal template for new design but also revealed the structure and function relationship of LCB1 inhibitor. As LCB1v8 was generated as a short peptide through chemical synthesis, rather than recombinant protein expression, it is amenable to further chemical modification, including the incorporation of non-proteinogenic amino acids, with the aim to stabilize the peptide against proteolytic degradation, as well as to improve the inhibitory strength and breadth.

Very recently, several studies also reported the successful development of truncated LCB1 peptides with the potent antiviral activity (Jawad et al., 2022; Khatri et al., 2022; Weissenborn et al., 2022). For example, Khatri and coworkers developed a thermostable dimeric helix-hairpin inhibitor through truncation of the third helix and optimization of the interhelical loop residues, which effectively prevented SARS-CoV-2 infection by dimerizing the S protein and protected hamsters from high dose viral challenge (Khatri et al., 2022). Alternatively, a smaller, stronger, more stable inhibitor was generated as a cyclic variant of the two-helix peptide (Weissenborn et al., 2022). For the first time, here we modified LCB1 as a helical lipopeptide and validated its high *in vitro* and *in vivo* virus-inhibitory efficacies. Impressively, LCB1v18 could efficiently protect transgenic mice from a lethal challenge when it was administrated as prophylaxis, whereas all the control mice administrated with a normal saline sham died from the virus challenge. Combined, these results underscore the promise of this class of peptides or lipopeptides that can strongly inhibit protein-protein interaction.

Last, we would like point out that our animal challenge studies were conducted prior to the emergence of diverse SARS-CoV-2 VOCs, so the effectiveness of LCB1-based lipopeptides should be further evaluated with emerging SARS-CoV-2 variants, especially using the currently circulating Omicron viruses for challenge. Although LCB1-based lipopeptides remained highly active in inhibiting VOCs and many other mutants, its further optimization is also needed to overcome the resistance phenotype. The other limitations of this class agents should be also considered, particularly in the light of current antiviral therapy. For example, the drug delivery route, patient compliance, as well as the difficulty of a lage-scale production and cost-effectiveness.

Author contributions

Y.Z., M.L., N.L., T.W., and X.H. performed the experiments. Y.Z., G. Z., and Y.He. analyzed the data. G.Z. and Y.H. supervised the study and wrote the paper with Y.Z. All authors read and approved the submitted version.

Disclosure statement

No potential conflict of interest was reported by the authors.

Declaration of competing interest

The authors declare that they have no known competing financial interests or personal relationships that could have appeared to influence the work reported in this paper.

Data availability

Data will be made available on request.

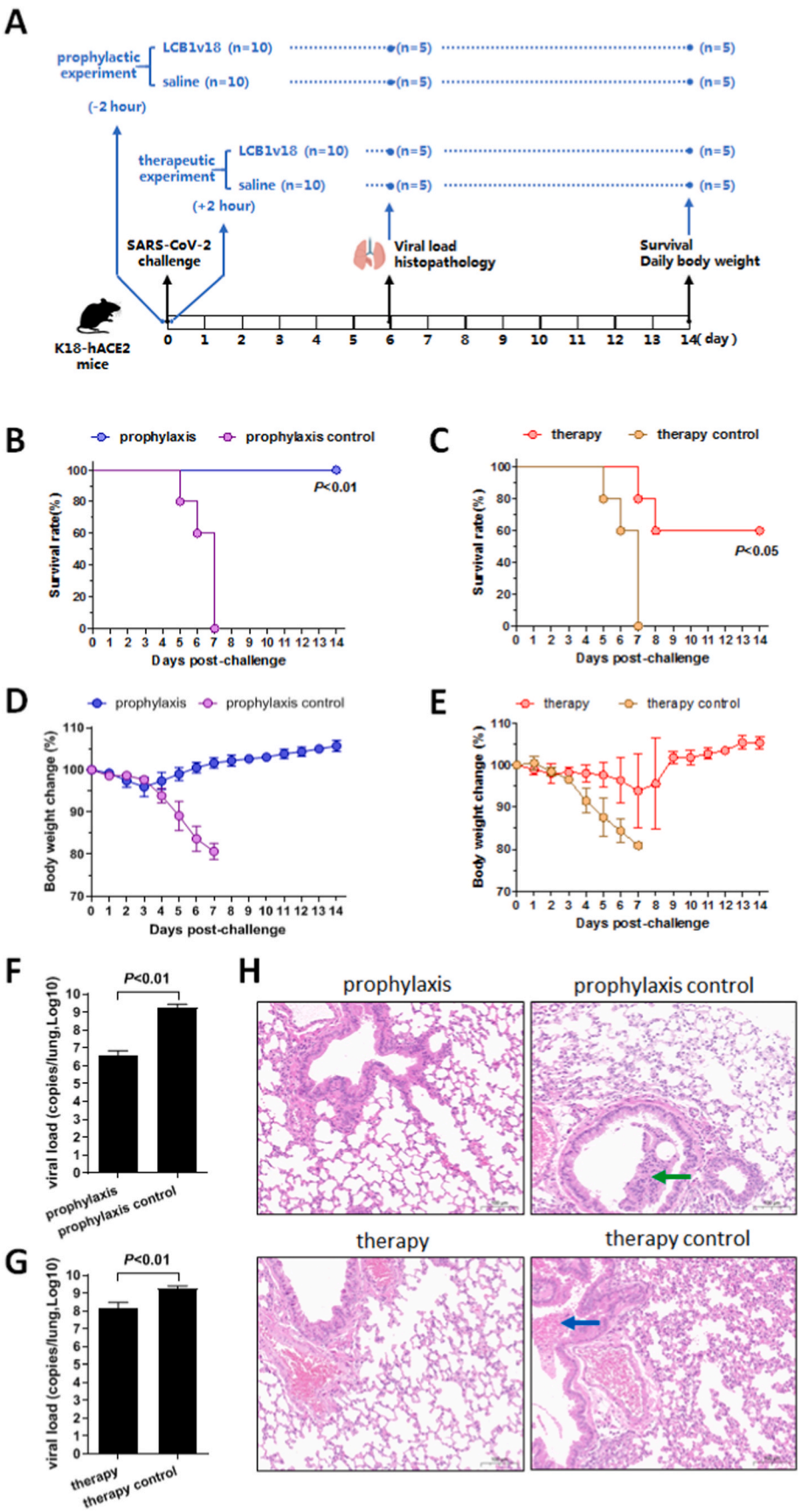

Fig. 6. LCB1v18 exhibits high prophylactic and therapeutic efficacies in K18-hACE2 mice. (**A**) Schematic map for evaluation on prophylactic and therapeutic effects of LCB1v18. (**B–C**) Mice were monitored for 14 days post-challenge to assess survival rate ($n = 5$). (**D-E**) The daily body weight was recorded post-challenge and the changes in body weight within 14 days was calculated. The data are expressed as the means ± SD (n = 5). (**F-G**) Viral load was detected in the mouse lung at day 6 post-infection. The data are expressed as the means ± SD (n = 5). (**H**) Histopathological changes in lung tissues of challenged mice. Representative images from mice received prophylactic-LCB1v18(a), LCB1v18-treatment (b) or controls (c & d) are shown. Lung tissue sections were stained with hematoxylin and eosin (H & E) and observed under light microscopy (scale bars, 100 μm). Blue and green arrows respectively showed quantities of erythrocytes and collapsed bronchiolar epithelium cells in bronchiole tubes.

Acknowledgements

We thank Linqi Zhang at the Tsinghua university (Beijing, China) for providing the plasmids that encode the mutant S proteins of SARS-CoV-2 VOCs. This work was supported by grants from the National Natural Science Foundation of China (822210040, 82230076) and the CAMS Innovation Fund for Medical Sciences (2021-I2M-1037).

References

Bowen, J.E., Addetia, A., Dang, H.V., Stewart, C., Brown, J.T., Sharkey, W.K., Sprouse, K. R., Walls, A.C., Mazzitelli, I.G., Logue, J.K., Franko, N.M., Czudnochowski, N., Powell, A.E., Dellota Jr., E., Ahmed, K., Ansari, A.S., Cameroni, E., Gori, A., Bandera, A., Posavad, C.M., Dan, J.M., Zhang, Z., Weiskopf, D., Sette, A., Crotty, S., Iqbal, N.T., Corti, D., Geffner, J., Snell, G., Grifantini, R., Chu, H.Y., Veesler, D., 2022. Omicron spike function and neutralizing activity elicited by a comprehensive panel of vaccines. Science, eabq0203.

Callaway, E., 2021. Heavily mutated Omicron variant puts scientists on alert. Nature 600, 21.

Cao, L., Goreshnik, I., Coventry, B., Case, J.B., Miller, L., Kozodoy, L., Chen, R.E., Carter, L., Walls, A.C., Park, Y.J., Strauch, E.M., Stewart, L., Diamond, M.S., Veesler, D., Baker, D., 2020. De novo design of picomolar SARS-CoV-2 miniprotein inhibitors. Science 370, 426–431.

Case, J.B., Chen, R.E., Cao, L., Ying, B., Winkler, E.S., Johnson, M., Goreshnik, I., Pham, M.N., Shrihari, S., Kafai, N.M., Bailey, A.L., Xie, X., Shi, P.Y., Ravichandran, R., Carter, L., Stewart, L., Baker, D., Diamond, M.S., 2021. Ultrapotent miniproteins targeting the SARS-CoV-2 receptor-binding domain protect against infection and disease. Cell Host Microbe 29, 1151–1161 e1155.

Chong, H., Zhu, Y., Yu, D., He, Y., 2018. Structural and functional characterization of membrane fusion inhibitors with extremely potent activity against HIV-1, HIV-2, and simian immunodeficiency virus. J. Virol. 92 e01088-01018.

de Vries, R.D., Schmitz, K.S., Bovier, F.T., Predella, C., Khao, J., Noack, D., Haagmans, B. L., Herfst, S., Stearns, K.N., Drew-Bear, J., Biswas, S., Rockx, B., McGill, G., Dorrello, N.V., Gellman, S.H., Alabi, C.A., de Swart, R.L., Moscona, A., Porotto, M., 2021. Intranasal fusion inhibitory lipopeptide prevents direct-contact SARS-CoV-2 transmission in ferrets. Science 371, 1379–1382.

Garcia-Beltran, W.F., Lam, E.C., St Denis, K., Nitido, A.D., Garcia, Z.H., Hauser, B.M., Feldman, J., Pavlovic, M.N., Gregory, D.J., Poznansky, M.C., Sigal, A., Schmidt, A.G., Iafrate, A.J., Naranbhai, V., Balazs, A.B., 2021. Multiple SARS-CoV-2 variants escape neutralization by vaccine-induced humoral immunity. Cell 184, 2372–2383 e2379.

Group, A.C.-T.f.I.w.C.-S., 2022. Efficacy and safety of two neutralising monoclonal antibody therapies, sotrovimab and BRII-196 plus BRII-198, for adults hospitalised with COVID-19 (TICO): a randomised controlled trial. Lancet Infect. Dis. 22, 622–635.

He, X., Hong, W., Pan, X., Lu, G., Wei, X., 2021. SARS-CoV-2 Omicron variant: characteristics and prevention. MedComm 2, 838–845.

Hoffmann, M., Arora, P., Gross, R., Seidel, A., Hornich, B.F., Hahn, A.S., Kruger, N., Graichen, L., Hofmann-Winkler, H., Kempf, A., Winkler, M.S., Schulz, S., Jack, H.M., Jahrsdorfer, B., Schrezenmeier, H., Muller, M., Kleger, A., Munch, J., Pohlmann, S., 2021. SARS-CoV-2 variants B.1.351 and P.1 escape from neutralizing antibodies. Cell 184, 2384–2393 e2312.

Hoy, S.M., 2022. Amubarvimab/romlusevimab: first approval. Drugs 82, 1327–1331.

Hunt, A.C., Case, J.B., Park, Y.J., Cao, L., Wu, K., Walls, A.C., Liu, Z., Bowen, J.E., Yeh, H. W., Saini, S., Helms, L., Zhao, Y.T., Hsiang, T.Y., Starr, T.N., Goreshnik, I., Kozodoy, L., Carter, L., Ravichandran, R., Green, L.B., Matochko, W.L., Thomson, C. A., Vogeli, B., Kruger, A., VanBlargan, L.A., Chen, R.E., Ying, B., Bailey, A.L., Kafai, N.M., Boyken, S.E., Ljubetic, A., Edman, N., Ueda, G., Chow, C.M., Johnson, M., Addetia, A., Navarro, M.J., Panpradist, N., Gale Jr., M., Freedman, B.S., Bloom, J.D., Ruohola-Baker, H., Whelan, S.P.J., Stewart, L., Diamond, M.S., Veesler, D., Jewett, M.C., Baker, D., 2022. Multivalent designed proteins neutralize SARS-CoV-2 variants of concern and confer protection against infection in mice. Sci. Transl. Med. 14, eabn1252.

Javanmardi, K., Chou, C.W., Terrace, C.I., Annapareddy, A., Kaoud, T.S., Guo, Q., Lutgens, J., Zorkic, H., Horton, A.P., Gardner, E.C., Nguyen, G., Boutz, D.R., Goike, J., Voss, W.N., Kuo, H.C., Dalby, K.N., Gollihar, J.D., Finkelstein, I.J., 2021. Rapid characterization of spike variants via mammalian cell surface display. Mol. Cell 81, 5099–5111 e5098.

Jawad, B., Adhikari, P., Cheng, K., Podgornik, R., Ching, W.Y., 2022. Computational design of miniproteins as SARS-CoV-2 therapeutic inhibitors. Int. J. Mol. Sci. 23.

Khatri, B., Pramanick, I., Malladi, S.K., Rajmani, R.S., Kumar, S., Ghosh, P., Sengupta, N., Rahisuddin, R., Kumar, N., Kumaran, S., Ringe, R.P., Varadarajan, R., Dutta, S., Chatterjee, J., 2022. A dimeric proteomimetic prevents SARS-CoV-2 infection by dimerizing the spike protein. Nat. Chem. Biol. 18, 1046-1055.

Kuzmina, A., Khalaila, Y., Voloshin, O., Keren-Naus, A., Boehm-Cohen, L., Raviv, Y., Shemer-Avni, Y., Rosenberg, E., Taube, R., 2021. SARS-CoV-2 spike variants exhibit differential infectivity and neutralization resistance to convalescent or post-vaccination sera. Cell Host Microbe 29, 522–528 e522.

Outlaw, V.K., Bovier, F.T., Mears, M.C., Cajimat, M.N., Zhu, Y., Lin, M.J., Addetia, A., Lieberman, N.A.P., Peddu, V., Xie, X., Shi, P.Y., Greninger, A.L., Gellman, S.H., Bente, D.A., Moscona, A., Porotto, M., 2020. Inhibition of coronavirus entry in vitro and ex vivo by a lipid-conjugated peptide derived from the SARS-CoV-2 spike glycoprotein HRC domain. mBio 11 e01935-01920.

Saito, A., Irie, T., Suzuki, R., Maemura, T., Nasser, H., Uriu, K., Kosugi, Y., Shirakawa, K., Sadamasu, K., Kimura, I., Ito, J., Wu, J., Iwatsuki-Horimoto, K., Ito, M., Yamayoshi, S., Loeber, S., Tsuda, M., Wang, L., Ozono, S., Butlertanaka, E.P., Tanaka, Y.L., Shimizu, R., Shimizu, K., Yoshimatsu, K., Kawabata, R., Sakaguchi, T., Tokunaga, K., Yoshida, I., Asakura, H., Nagashima, M., Kazuma, Y., Nomura, R., Horisawa, Y., Yoshimura, K., Takaori-Kondo, A., Imai, M., Genotype to Phenotype Japan, C., Tanaka, S., Nakagawa, S., Ikeda, T., Fukuhara, T., Kawaoka, Y., Sato, K., 2022. Enhanced fusogenicity and pathogenicity of SARS-CoV-2 Delta P681R mutation. Nature 602, 300–306.

Shrestha, L.B., Foster, C., Rawlinson, W., Tedla, N., Bull, R.A., 2022. Evolution of the SARS-CoV-2 omicron variants BA.1 to BA.5: implications for immune escape and transmission. Rev. Med. Virol. 32, e2381.

Sun, S., He, L., Zhao, Z., Gu, H., Fang, X., Wang, T., Yang, X., Chen, S., Deng, Y., Li, J., Zhao, J., Li, L., Li, X., He, P., Li, G., Li, H., Zhao, Y., Gao, C., Lang, X., Wang, X., Fei, G., Li, Y., Geng, S., Gao, Y., Wei, W., Hu, Z., Han, G., Sun, Y., 2021. Recombinant vaccine containing an RBD-Fc fusion induced protection against SARS-CoV-2 in nonhuman primates and mice. Cell. Mol. Immunol. 18, 1070–1073.

Walls, A.C., Park, Y.J., Tortorici, M.A., Wall, A., McGuire, A.T., Veesler, D., 2020. Structure, function, and antigenicity of the SARS-CoV-2 spike glycoprotein. Cell 181, 281–292 e286.

Wang, P., Nair, M.S., Liu, L., Iketani, S., Luo, Y., Guo, Y., Wang, M., Yu, J., Zhang, B., Kwong, P.D., Graham, B.S., Mascola, J.R., Chang, J.Y., Yin, M.T., Sobieszczyk, M., Kyratsous, C.A., Shapiro, L., Sheng, Z., Huang, Y., Ho, D.D., 2021. Antibody resistance of SARS-CoV-2 variants B.1.351 and B.1.1.7. Nature 593, 130–135.

Weissenborn, L., Richel, E., Huseman, H., Welzer, J., Beck, S., Schafer, S., Sticht, H., Uberla, K., Eichler, J., 2022. Smaller, stronger, more stable: peptide variants of a SARS-CoV-2 neutralizing miniprotein. Int. J. Mol. Sci. 23.

Wrapp, D., Wang, N., Corbett, K.S., Goldsmith, J.A., Hsieh, C.L., Abiona, O., Graham, B. S., McLellan, J.S., 2020. Cryo-EM structure of the 2019-nCoV spike in the prefusion conformation. Science 367, 1260–1263.

Wu, T., Zhu, Y., Liu, N., Hu, Y., Chong, H., He, Y., 2022. Resistance profile and mechanism of SARS-CoV-2 variants to LCB1 inhibitor targeting the spike receptor-binding motif. Front. Microbiol. 13, 1022006.

Xue, J., Chong, H., Zhu, Y., Zhang, J., Tong, L., Lu, J., Chen, T., Cong, Z., Wei, Q., He, Y., 2022. Efficient treatment and pre-exposure prophylaxis in rhesus macaques by an HIV fusion-inhibitory lipopeptide. Cell 185, 131–144 e118.

Yu, D., Zhu, Y., Jiao, T., Wu, T., Xiao, X., Qin, B., Chong, H., Lei, X., Ren, L., Cui, S., Wang, J., He, Y., 2021a. Structure-based design and characterization of novel fusion-inhibitory lipopeptides against SARS-CoV-2 and emerging variants. Emerg. Microb. Infect. 10, 1227–1240.

Yu, D., Zhu, Y., Yan, H., Wu, T., Chong, H., He, Y., 2021b. Pan-coronavirus fusion inhibitors possess potent inhibitory activity against HIV-1, HIV-2, and simian immunodeficiency virus. Emerg. Microb. Infect. 10, 810–821.

Zhang, J., Xiao, T., Cai, Y., Lavine, C.L., Peng, H., Zhu, H., Anand, K., Tong, P., Gautam, A., Mayer, M.L., Walsh Jr., R.M., Rits-Volloch, S., Wesemann, D.R., Yang, W., Seaman, M.S., Lu, J., Chen, B., 2021. Membrane fusion and immune evasion by the spike protein of SARS-CoV-2 Delta variant. Science 374, 1353–1360.

Zhu, Y., Chong, H., Yu, D., Guo, Y., Zhou, Y., He, Y., 2019. Design and characterization of cholesterylated peptide HIV-1/2 fusion inhibitors with extremely potent and long-lasting antiviral activity. J. Virol. 93 e02312-02318.

Zhu, Y., Dong, X., Liu, N., Wu, T., Chong, H., Lei, X., Ren, L., Wang, J., He, Y., 2022a. SARS-CoV-2 fusion-inhibitory lipopeptides maintain high potency against divergent variants of concern including Omicron. Emerg. Microb. Infect. 11, 1819–1827.

Zhu, Y., Hu, Y., Liu, N., Chong, H., He, Y., 2022b. Potent inhibition of diverse Omicron sublineages by SARS-CoV-2 fusion-inhibitory lipopeptides. Antivir. Res. 208, 105445.

Zhu, Y., Yu, D., Hu, Y., Wu, T., Chong, H., He, Y., 2021. SARS-CoV-2-derived fusion inhibitor lipopeptides exhibit highly potent and broad-spectrum activity against divergent human coronaviruses. Signal Transduct. Targeted Ther. 6, 294.

Zhu, Y., Yu, D., Yan, H., Chong, H., He, Y., 2020. Design of potent membrane fusion inhibitors against SARS-CoV-2, an emerging coronavirus with high fusogenic activity. J. Virol. 94 e00635-00620.